Adsorption (2013) 19:407–422
DOI 10.1007/s10450-012-9463-6

Adsorption and diffusion of nitrogen, methane and carbon dioxide in aluminophosphate molecular sieve $AlPO_4$-11

J. A. Delgado · V. I. Águeda · M. A. Uguina · J. L. Sotelo · Paz Fernández

Received: 8 September 2012 / Accepted: 21 December 2012 / Published online: 8 January 2013

Abstract The knowledge about the adsorption and diffusion properties (specially about diffusion) of aluminophosphate molecular sieves is very scarce in the literature. These materials offer interesting properties as adsorbents as they have a polar framework and do not contain charge-balancing cations. In this work, the adsorption isotherms of nitrogen, methane and carbon dioxide over an $AlPO_4$-11 sample synthesized in our laboratories have been measured with a volumetric method at 25, 35, 50 and 65 °C over a pressure range up to 110 kPa. The adsorption capacities of each gas are determined by the strength of interaction with the pore surface (carbon dioxide > methane > nitrogen). The equilibrium selectivity to carbon dioxide is quite high with respect to other adsorbents without cations due to the polarity of the aluminophosphate framework. The adsorption Henry's law constants and diffusion time constants of nitrogen, methane and carbon dioxide in the synthesized $AlPO_4$-11 material have been measured from pulse experiments. A pressure swing adsorption (PSA) process for recovering methane from a carbon dioxide/methane mixture (resembling biogas) has been designed using a dynamic model where the measured adsorption equilibrium and kinetic information has been incorporated. The simulation results show that the proposed process could be simpler than other PSA processes for biogas upgrading based on cation-containing molecular sieves such as 13X zeolite, as it can treat the biogas at atmospheric pressure, and it requires a lower pressure ratio, to produce high purity methane with high recovery.

J. A. Delgado (✉) · V. I. Águeda · M. A. Uguina · J. L. Sotelo · P. Fernández
Department of Chemical Engineering, Universidad Complutense de Madrid, 28040 Madrid, Spain
e-mail: jadeldob@quim.ucm.es

Keywords Carbon dioxide · Methane · Nitrogen · $AlPO_4$-11 · Adsorption · Diffusion · Pressure swing adsorption

List of symbols

b	Adsorption affinity (Pa^{-1})
b_0	Pre exponential constant (Eq. 1) (Pa^{-1})
c	Adsorptive concentration in the gas phase (mol m^{-3})
C	Total gas concentration (mol m^{-3})
$c_{p,g}$	Gas heat capacity at constant pressure (J mol^{-1} K^{-1})
$c_{p,s}$	Adsorbent heat capacity (J kg^{-1} K^{-1})
$c_{v,g}$	Gas heat capacity at constant volume (J mol^{-1} K^{-1})
D_c	Intracrystalline diffusivity (m^2 s^{-1})
D_L	Axial dispersion coefficient (m^2 s^{-1})
D_m	Molecular diffusivity (m^2 s^{-1})
f_{pulse}	Function defined in Eq. (13)
h_{ext}	Wall to air heat transfer coefficient (W m^{-2} K^{-1})
h_w	Gas to wall heat transfer coefficient (W m^{-2} K^{-1})
K_c	Dimensionless Henry's law constant
k_f	External mass transfer coefficient (m s^{-1})
k_{macro}	Combined mass transfer coefficient in the external film and the macropores (m s^{-1})
k_s	LDF mass transfer coefficient (s^{-1})
L	Bed length (m)
l	Wall thickness (m)
n	Adsorbed concentration (mol kg^{-1})
n_{max}	Maximal adsorbed concentration (mol kg^{-1})
p	Adsorptive pressure (Pa)
P	Pressure (Pa)
q	Adsorbed concentration (mol m^{-3})
Q	Volumetric flow rate (m^3 s^{-1})

R	Gas constant (J mol^{-1} K^{-1})
r_c	Half diffusion length in the spherulites (m)
r^2	Coefficient of determination
Re	Particle Reynolds number
R_l	Bed radius (m)
R_p	Size of the adsorbent particle (m)
S_{bed}	Bed cross-section (m^2)
Sc	Schmidt number
T	Temperature (K)
t	Time (s)
T_w	Wall temperature (K)
u	Superficial velocity (m s^{-1})
v_0	Interstitial velocity (m s^{-1})
V_D	Plug-flow volume (m^3)
V_T	Tank volume (m^3)
x	Dimensionless axial coordinate
x_r	Dimensionless radial coordinate
z	Axial coordinate (m)
$-\Delta H_{ads}$	Adsorption enthalpy (J mol^{-1})

Greek symbols

y	Mole fraction in the gas phase
ε	Bed voidage fraction between adsorbent particles
ε_{macro}	Pellet macroporosity
ε_p	Particle porosity
λ	Axial heat dispersion coefficient (W m^{-1} K^{-1})
μ	First moment of the pulse response, gas viscosity (Pa s)
ρ_c	Crystal density (kg m^{-3})
ρ_g	Gas density (kg m^{-3})
ρ_p	Particle density (kg m^{-3})
τ	Tortuosity

1 Introduction

The synthesis of aluminophosphate molecular sieves ($AlPO_4$s) was first reported in 1982 (Wilson et al. 1982a, b. These materials are formed by tetrahedrally coordinated AlO_4 and PO_4, and have no need for charge-balancing cations. A large number of silicoaluminophosphate ($SAPO_4$) analogs have also been synthesized. The rich variety of pore structures, both cavities and channels, as well as the cation sites that can be exchanged in the $SAPO_4$ analogs, offer promising opportunities for their use as new sorbents for separations (Yang 2003). Among them, the AEL structure of $AlPO_4$-11 is particularly interesting. It has 10-membered ring channels with pore dimensions of 0.63 × 0.39 nm (Baerlocher et al. 2001), which falls within the size of medium-pore zeolites, such as ZSM-5. The adsorption selectivity of $AlPO_4$-11 towards the orto-isomer in a mixture of xylenes has been investigated by Lucena et al. (2006). $AlPO_4$-11 and its corresponding substituted materials have been investigated as catalysts in the methanol-to-olefin conversion (Zhu et al. 2000) and the hydroisomerisation of n-paraffins (Walendziewski and Pniak 2003). Different methods of $AlPO_4$-11 and $SAPO_4$-11 synthesis have been proposed to change the size and the extracrystalline pore size distribution of the crystals (Zhu et al. 2001; Wang et al. 2009; Fu et al. 2011).

The knowledge about the adsorption and diffusion properties (specially about diffusion) of aluminophosphate molecular sieves is very scarce in the literature. Some molecular simulation studies have been carried out using $AlPO_4$-11 as adsorbent (Zhang et al. 2007; Lucena et al. 2006). However, the experimental measurement of adsorption and diffusion properties is very important in the design of the adsorption separation processes, and it is also required to validate the prediction of these properties by molecular simulation. Predescu et al. (1997) measured the adsorption isotherms of nitrogen, methane and carbon monoxide on several aluminophosphate molecular sieves ($AlPO_4$-11, $AlPO_4$-17 and $AlPO_4$-18), but nor the adsorption enthalpy nor the diffusion properties of these gases were provided.

One important characteristic of aluminophosphate molecular sieves is the absence of cations in the zeolitic pores. When conventional cation-containing aluminosilicate molecular sieves are used in the separation of gaseous mixtures containing polar molecules, a common problem is the difficulty in the regeneration of the spent adsorbent due to the strong interaction between the polar adsorbates and the cations in the zeolitic pores. This problem exists in the upgrading of biogas (mainly composed of carbon dioxide and methane) by pressure swing adsorption (PSA) using 13X zeolite (which contains Na cations), where high pressure ratios are required due to the highly favorable character of the carbon dioxide isotherm (highest pressure/lowest pressure in the cycle = 48–80, Sircar et al. 1988; Grande and Rodrigues 2007). Recently, Santos et al. (2011) have proposed a new cycle configuration which can reduce the pressure ratio of a PSA cycle for biogas upgrading (based on 13X zeolite or a carbon molecular sieve) to 13, but still a feed pressure of 4 bar is required, and it is also required to increase the temperature up to 323 K, to reduce the steepness of the carbon dioxide isotherm.

In this separation, the regeneration can be simpler using an aluminophosphate molecular sieve as adsorbent, because the carbon dioxide-cation interaction is absent. Biogas is usually produced in anaerobic digestors, where the operating pressure rarely exceeds 24 in H_2Og (1.06 bar), and can be used without compression (Wilke et al. 2012). Separating methane with $AlPO_4$-11 using a feed pressure of 1 bar can be advantageous, as feed compression is not required.

The objectives of this work are the following: (1) to measure the adsorption isotherms of nitrogen, methane and carbon dioxide on aluminophosphate molecular sieve $AlPO_4$-11 at four temperatures (25, 35, 50 and 65 °C) up to 110 kPa (2) to measure the diffusion parameters of these gases at zero loading in this material, and (3) to evaluate the potential performance of $AlPO_4$-11 in the carbon dioxide-methane separation by PSA using the adsorption equilibrium and kinetic data measured in this work to design this process.

2 Experimental section

2.1 Synthesis and characterization of $AlPO_4$-11

The synthesis of $AlPO_4$-11 has been carried out in a 250 ml flask using the following molar composition of the precursor gel (Wilson et al. 1982b; Lok et al. 1984):1 Al_2O_3:1 P_2O_5:1 di-*n*-propylamine:50 H_2O. Measured amounts of phosphoric acid (20.5 g) and water (20 g) are mixed and stirred vigorously. To this mixture, pseudobohemite (16.9 g) is added slowly (during 2 h), as a source of aluminum. The resulting mixture is kept under stirring during 1 h more. The template (di-*n*-propylamine) (9.1 g) is added drop by drop to this mixture, and finally, water is added up (47.3 g) to get the desired proportion, keeping the mixture under stirring half an hour more. The precursor gel is put in a Teflon reaction vessel (100 ml), and heated at 180 °C in a microwave oven (MLS-1200 MEGA) for 15 min to induce the crystallization. After this, the vessel is cooled and its content is centrifuged to separate the solids, which are washed with Milli-Q water, dried at 100 °C, and finally calcined at 600 °C for 1 h.

The crystalline structure of the synthesized material was confirmed by XRD (Phillips, X'PERT MPD model), and its composition was determined by XRF (Phillips, AXIOS model). The morphology and the size of crystals were determined by SEM (JEOL, JSM-6400 model). The textural properties were measured by nitrogen porosimetry (Micromeritics ASAP2020) and mercury porosimetry (Thermo Finnigan Pascal 140 model).

2.2 Measurement of the adsorption isotherms

All the gases used in this work had purity higher than 99.5 %, supplied by Praxair. The adsorption isotherms of nitrogen, methane and carbon dioxide on the synthesized material have been measured in a volumetric equipment (Micromeritics ASAP2000). The glass tube loaded with the sample (3 g) is surrounded with a jacket connected to a thermosttated bath to measure the isotherms at different temperatures.

2.3 Diffusion measurements

A scheme of the experimental setup used to carry out the diffusion measurements is shown in Fig. 1. The flow of the selected gas (helium or nitrogen) is controlled with mass flow controllers. The stainless-steel column (i.d. = 9 mm, 25 cm long) containing the adsorbent bed is surrounded by two stainless-steel spiral tubes (1/8″), one of them to preheat the feed gas (shown separately for simplicity in Fig. 1), and the other (not shown) to control the bed temperature with a thermostatted bath. The column and the surrounding spiral tubes are covered by an electrical co-axial furnace, so that the bed temperature can be controlled between 25 and 600 °C. The bed temperature is measured by two thermocouples in contact with the adsorbent. Two glass hollow sticks reduce the dead volume outside the bed, through which two thermocouples are inserted. Small layers of glass wool are placed between the three column sections (glass stick-adsorbent-glass stick). All the connections are made of Teflon and stainless-steel tubing (1/8″). The gas flow rate at the bed exit was measured with a bubble meter.

The experiments for the adsorption and diffusion measurements were performed by injecting small amounts of gas (0.5 ml) in a stream of carrier gas (helium or nitrogen), passing through the bed (∼1 g of adsorbent) with controlled temperature. The bed properties are given in Table 1. The value of the porosity between particles was calculated as 1- bed density/particle density, where both parameters were measured experimentally. The bed density was measured in a graduated cylinder of the same diameter as the column used in the pulse experiments, resulting in 0.625 g cm^{-3}. The particle density (0.882 g cm^{-3}) was measured by Hg displacement, using a commercial Hg porosimeter (Thermo Finnigan Pascal 140 model). The

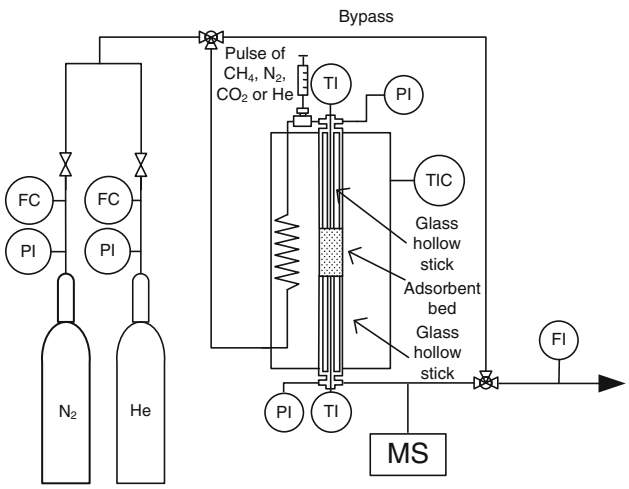

Fig. 1 Scheme of the setup for diffusion measurements

Table 1 Bed properties in the pulse experiments

Length	0.025 m
Mass	0.995 g
Porosity between particles	0.29
Diameter	0.009 m

relatively low value of the bed porosity (0.29) indicates that the adsorbent particles pack well in the bed.

The pulse responses are recorded by a mass spectrometer (Balzers ThermoStar). Each pulse was repeated three times to check the reproducibility. Pressure drop along the bed was not detectable in the pulse experiments.

3 Results and discussion

3.1 Characterization of the synthesized $AlPO_4$-11

Table 2 summarizes the physicochemical properties of the synthesized material. The P/Al ratio measured experimentally is close to 1, the theoretical value for aluminophosphate molecular sieves. Figure 2 shows the XRD diffraction pattern of the synthesized material, which corresponds to the AEL structure of $AlPO_4$-11 (Baerlocher et al. 2001). The pore volume and the surface area measured by nitrogen porosimetry come from the micropores in this structure. The relatively high Hg intrusion volume is due to a significant amount of meso- and macropores in the adsorbent, as indicated by the pore size distribution measured with this technique (Fig. 3).

Figure 4 shows SEM photographs of the synthesized material. It is observed that the adsorbent consist of spherulites (polycrystalline aggregates) with sizes ranging between 2 and 7 μm approximately, which form loosely aggregated bigger particles (floccules). The measurement of the particle size distribution of the individual spherulites is quite difficult, as the spherulites are aggregated. The size of these floccules is of the order of 10–20 μm, estimated from the SEM images. It is important to note that the accurate particle size distribution of the floccules is not important for measuring the diffusion properties in the synthesized $AlPO_4$-11 material, because the mass transfer resistance in the extracrystalline porosity in the floccules is negligible, as it is discussed later. Taking into account that the Hg intrusion pore size distribution indicates a high proportion of pores with diameters around 2 μm, it is deduced that these pores mainly come from the interstices between the spherulites. Therefore, the adsorbent particles (floccules) have a bidisperse pore structure, including the macropores between spherulites and the intracrystalline porosity. The small fraction of mesoporosity in the synthesized material detected by Hg porosimetry (with pore radius <10 nm) may be due to the presence of some extracrystalline internal porosity in the spherulites. The presence of mesoporosity is confirmed by the hysteresis of the N_2 adsorption isotherm in the synthesized material (Fig. 3b). As the spherulites are not perfectly dense crystals, but they are formed by intertwined crystallites (as it is shown in the SEM images in Fig. 4), they can have some internal mesoporosity in the zones where the crystallites do not pack perfectly.

3.2 Adsorption isotherms of nitrogen, methane and carbon dioxide on $AlPO_4$-11

Figure 5 presents the experimental adsorption isotherms of nitrogen, methane and carbon dioxide on the synthesized $AlPO_4$-11 material at different temperatures. The adsorption affinity follows the order: carbon dioxide > methane > nitrogen. It is observed that the molecular size (estimated as kinetic diameter, methane, 0.38 nm > nitrogen, 0.36 nm > carbon dioxide, 0.33 nm) does not determine the adsorption affinity because all the molecules are smaller than the pore openings of $AlPO_4$-11. Carbon dioxide adsorbs more than methane due to its higher polarizability, resulting in a stronger interaction by dispersion forces, and to its permanent quadrupole moment, which can interact with the local electric field gradient coming from the lower electronegativity of Al atom with respect to P atom. Methane adsorbs more than nitrogen in spite of its lack of electric moments, because of its higher polarizability.

The experimental data for the three gases at different temperatures were fitted with the Langmuir model [Eq. (1)], because it allows describing the adsorption equilibrium of gas mixtures easily (Yang 2003), which was

Table 2 Physicochemical properties of the synthesized $AlPO_4$-11 material

P/Al (molar)	Particle density (g cm^{-3})	Hg intrusion volume (cm^3 g^{-1})	Particle porosity[a]	Crystal density[b] (g cm^{-3})	Pore volume N_2 77 K (saturation) (cm^3 g^{-1})	Micropore volume (t-plot) (cm^3 g^{-1})	BET surface area (m^2 g^{-1})
0.91	0.882	0.751	0.66	2.612	0.22	0.068	175

[a] Considering the void volume estimated by Hg porosimetry only

[b] Excluding the Hg intrusion volume from the particle density

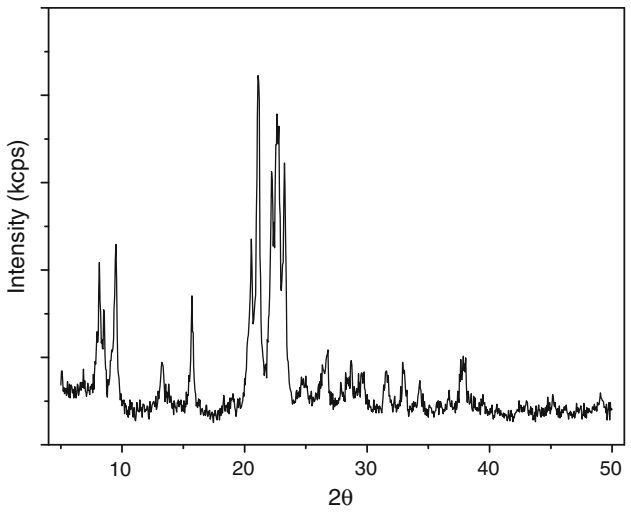

Fig. 2 XRD pattern of the as-synthesized $AlPO_4$-11

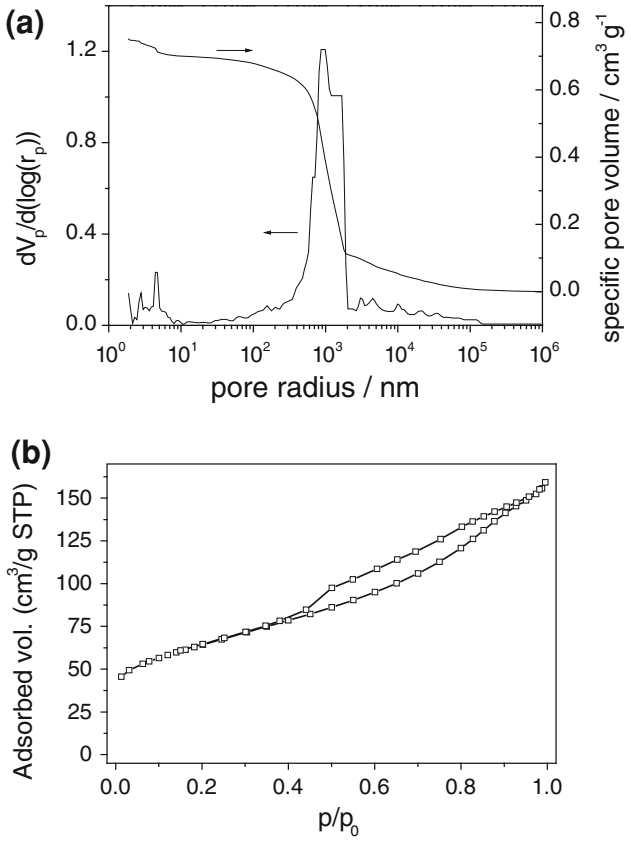

Fig. 3 Porosimetry results of the as-synthesized $AlPO_4$-11. **a** Pore size distribution of the as-synthesized $AlPO_4$-11 measured with Hg porosimetry. **b** N_2 adsorption isotherm at 77 K

required to simulate the separation of carbon dioxide-methane mixtures by PSA:

$$n = \frac{n_{\max} bp}{1 + bp} \quad b = b_0 \exp\left(\frac{-\Delta H_{ads}}{RT}\right) \tag{1}$$

where n is the adsorbed concentration (in mol kg^{-1}), b is the adsorption affinity, n_{max} is the maximum adsorption capacity, b_0 is the pre exponential constant of the adsorption affinity, and $-\Delta H_{ads}$ is the heat of adsorption. The fitting results are presented in Table 3, and a comparison between the experimental and theoretical isotherms is shown in Fig. 5. The errors of the estimated parameter values (Table 3) are significant due to the strong correlation between n_{max} and b_0. However, if these parameters are used in the studied pressure and temperature ranges (0–110 kPa and 25–65 °C) they result in a satisfactory reproduction of the experimental data, as it is shown in Fig. 5.

It is observed that the Langmuir model gives a good description of the adsorption isotherms of nitrogen and methane in the whole pressure range, whereas for carbon dioxide a good fit is only obtained for pressures above 5 kPa. It is probable that the adsorbent is energetically heterogeneous for carbon dioxide at low pressures, suggesting an uneven distribution of the electric field gradient in the pores, which can interact with the strong quadrupole moment of carbon dioxide molecules. The estimated values of the adsorption heats, particularly for carbon dioxide, must be interpreted as average values in the whole studied pressure and temperature range, which are useful for design purposes. The adsorption heats follow the order of the adsorption affinity discussed previously.

Assuming that the extended Langmuir equation can be used to describe the binary adsorption isotherms in carbon dioxide/methane mixtures, the adsorbent equilibrium selectivity for carbon dioxide is estimated as the ratio $(n_{max}\, b)_{CO2}/(n_{max}\, b)_{CH4}$, (Yang 2003). This gives a value of 6.13 for $AlPO_4$-11, a rather high value in comparison with other adsorbents that do not contain cations. For silicalite, this parameter (estimated as the ratio of Henry's law constants) at 25 °C is about 5 (Dunne et al. 1996), and for activated carbon is about 3 (Valenzuela and Myers 1989). The higher carbon dioxide selectivity comes from the higher polarity of the $AlPO_4$-11 structure.

3.3 Estimation of the adsorption and diffusion parameters from pulse experiments

The adsorption Henry's law constants and diffusion time constants of nitrogen, methane and carbon dioxide in the synthesized $AlPO_4$-11 material have been measured from pulse experiments. Pulses of helium (considered as a non-adsorbing gas, with nitrogen as carrier) were also obtained to take into account the void volume in the installation in the calculations, and to model the effect of the overall dispersion on the experimental pulse signal. The measurements were carried out with two different carrier gas flow rates. The experimental conditions are given in

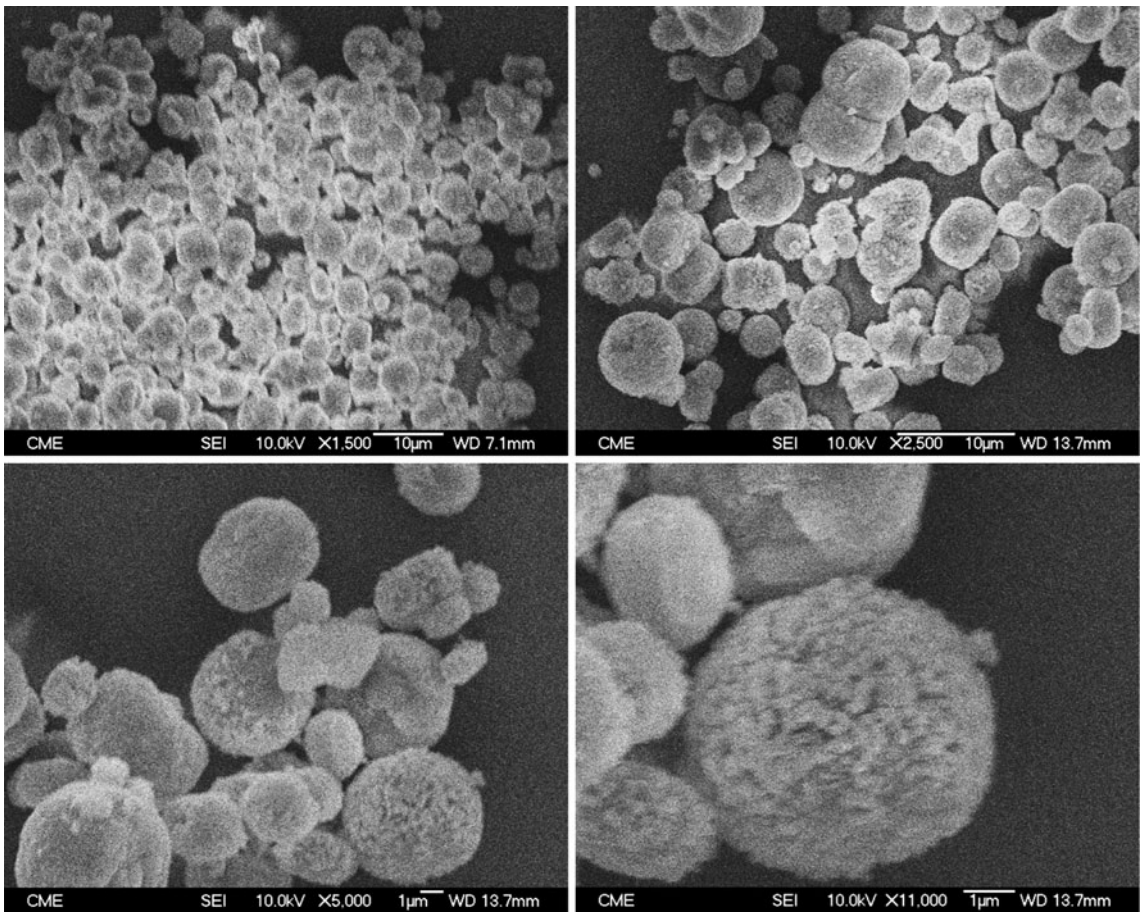

Fig. 4 SEM photographs of the as-synthesized $AlPO_4$-11

Tables 4 and including the total flow of gas, and the experimental pulse responses are presented in Fig. 6, where the baselines have been displaced for the sake of clarity. The pulse responses are normalized (the area below each pulse response is 1).

By applying the method of moments (Karger and Ruthven 1992) to the experimental pulse responses, the value of the adsorption Henry's law constant of the studied adsorptive can be extracted from the first moment of the experimental curve [Eq. (2)]:

$$\mu = \int_0^{t_\infty} (\text{normalized signal}) \cdot t dt \tag{2}$$

where t is time, starting from the moment of the pulse injection. The dimensionless Henry's law constant of a predetermined gas is given by:

$$K_c = \frac{v_0}{L} \frac{\varepsilon(\mu_{gas} - \mu_{He})}{(1-\varepsilon)(1-\varepsilon_p)} \tag{3}$$

where v_0 is the interstitial velocity, L is the bed length, ε is the bed void fraction between particles (Table 1), and ε_p is the particle porosity (Table 2). The value of μ_{He} is calculated from the helium pulse with the same values of carrier flow rate and temperature as those of the predetermined gas.

To compare K_c with the Henry's law constant deduced from the Langmuir model ($n_{max}b$), it must be divided by $\rho_c RT$, where the ρ_c is the crystal density (Table 2). Equation (3) was employed to estimate the Henry's law constant in each pulse experiment, and a comparison with the value predicted with the Langmuir model is presented in Table 4. It is observed the Henry's law constant measured by both methods are in good agreement, indicating that the estimated values of this parameter are reliable.

To estimate the diffusion time constant of each gas from the experimental pulse responses, it is necessary to subtract the effect of other mass transfer phenomena apart from the intracrystalline diffusion. It was found that a plug flow and tank-in-series model was adequate to describe the effect of dispersion on the pulse response. A schematic representation of the flow pattern assumed is presented in Fig. 7, where Q is the carrier gas flow rate (measured at laboratory conditions), V_D is the portion of void volume with plug flow, and V_T is the volume of each tank where perfect mixing is considered. The theoretical model used for simulating the pulse responses

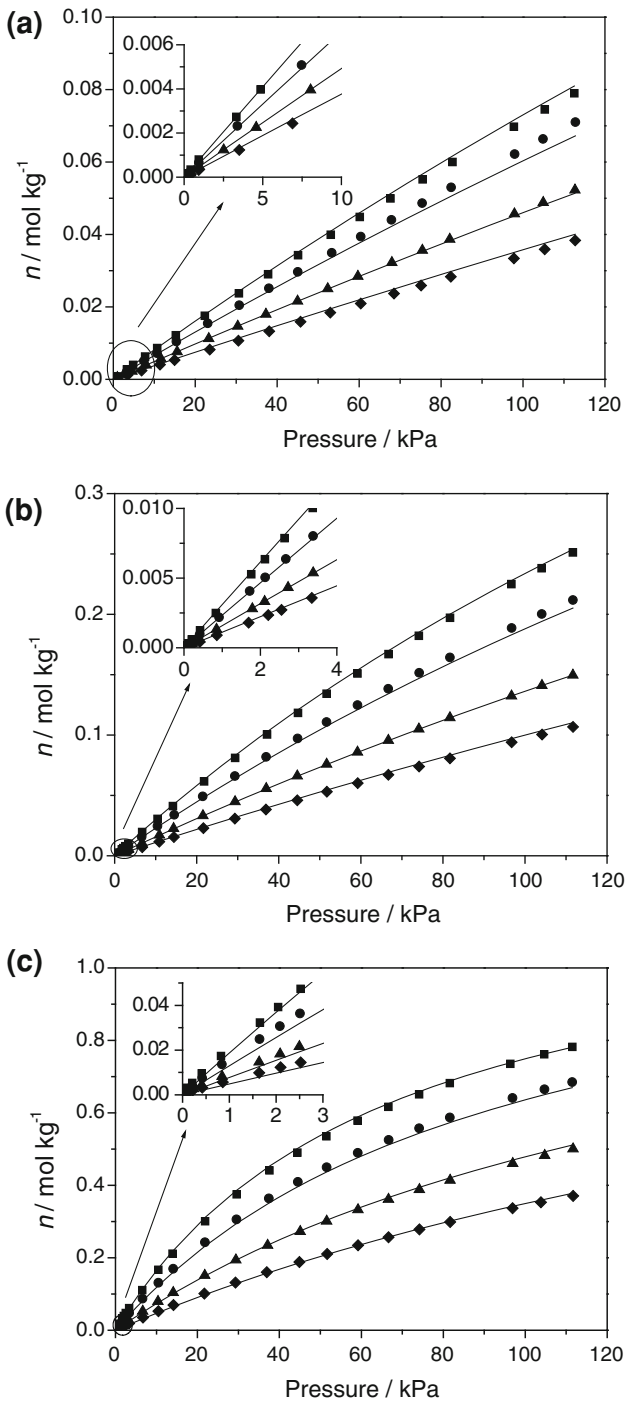

Fig. 5 Adsorption isotherms on $AlPO_4$-11. *Squares*, 25 °C; *circles*, 35 °C; *triangles*, 50 °C; *diamonds*, 65 °C. Lines depict the Langmuir model. **a** Nitrogen. **b** Methane. **c** Carbon dioxide

consists of the mass balances around each element in the system, interconnected according to the flow pattern. A good description of the experimental helium pulses was obtained with four tanks, two before and two after the bed. Other model assumptions are the following:

1. The gas velocity is constant along the bed
2. The adsorbent bed is isothermal
3. Radial concentration gradients are negligible
4. The adsorption isotherm is linear for all the adsorbates in the studied conditions
5. The external mass transfer resistance and the resistance in macropores is described with a linear driving force considering both resistances in series.

Assumption (2) is justified because no variation of the bed temperature was observed in the pulse experiments (measured experimentally), and assumptions (1) and (4) are justified because the average concentration of the adsorbing gases in the bed is rather low (below 3, 2 and 1 % v/v for nitrogen, methane and carbon dioxide, respectively, estimated with the theoretical model), which falls within the linear region of the adsorption isotherms (Fig. 5). Assumptions (3) and (5) were included because they simplify the model resolution.

The mass balance in the fixed bed is,

$$\frac{\partial c}{\partial t} = \frac{D_L}{L^2}\frac{\partial^2 c}{\partial x^2} - \frac{v_0}{L}\frac{\partial c}{\partial x} - \frac{3}{R_p}\frac{1-\varepsilon}{\varepsilon}k_{macro}(c - c_{macro}) \tag{4}$$

where c is the adsorptive concentration in the gas phase, t is time, D_L is the axial dispersion coefficient, L is the bed length, x is the dimensionless axial coordinate, ε is the bed porosity between particles (floccules), R_p is the half diffusion length of the floccules (taken as 15 μm), k_{macro} is the mass transfer coefficient describing the total extracrystalline resistance, and c_{macro} is the average concentration in the macropores. The value of k_{macro} is estimated from the following equation:

$$k_{macro} = \left(\frac{1}{\frac{5D_m\varepsilon_p}{\tau R_p}} + \frac{1}{k_f}\right)^{-1} \tag{5}$$

where D_m is the molecular diffusivity of the studied gas in the carrier, τ is the tortuosity of the macropores (taken as 3), and k_f is the external mass transfer coefficient, estimated with a literature correlation (Dwivedi and Upadhyay 1977):

$$k_f = \frac{u}{\varepsilon Sc^{2/3}}\left(\frac{0.765}{Re^{0.82}} + \frac{0.365}{Re^{0.386}}\right) \tag{6}$$

where u is the superficial velocity, Re is the particle Reynolds number, and Sc is the Schmidt number, calculated with the density and the viscosity of the carrier. The axial dispersion coefficient was estimated with an expression available in the literature for beds of small particles (<1–2 mm) (Suzuki 1990).

$$D_L = \frac{D_m}{2.5\varepsilon} \tag{7}$$

where D_m is the molecular diffusivity of the adsorptive in the carrier gas. The interstitial velocity is calculated as:

Table 3 Fitting results of the Langmuir model in $AlPO_4$-11

Gas	n_{max} (mol kg^{-1})	b_0 (Pa^{-1})	$-\Delta H_{ads}$ (kJ mol^{-1})	$n_{max}\,b$ at 25 °C (mol kg^{-1} Pa^{-1})	r^2
N_2	0.638 ± 0.2[a]	(1.82 ± 0.5) × 10^{-9}	16.28 ± 0.6	8.33 × 10^{-7}	0.998
CH_4	0.948 ± 0.07	(5.81 ± 0.8) × 10^{-10}	21.41 ± 0.4	3.13 × 10^{-6}	0.999
CO_2	1.237 ± 0.02	(1.55 ± 0.3) × 10^{-10}	28.51 ± 0.5	1.92 × 10^{-5}	0.999

[a] The 95 % confidence intervals were estimated with Origin 6.0® program

Table 4 Experimental conditions for the pulse experiments with methane, nitrogen and carbon dioxide in $AlPO_4$-11, and estimated adsorption and diffusion parameters

Injected gas	Total flow rate (10^{-6} m^3 s^{-1})	T (K)	$K_c/(\rho_c\,RT)$ (mol kg^{-1} Pa^{-1})	[a]$n_{max}b$ (mol kg^{-1} Pa^{-1})	D_c/r_c^2 (s^{-1})	r^2
N_2	0.51	298	8.8 × 10^{-7}	8.3 × 10^{-7}		
N_2	1.03	298	9.2 × 10^{-7}	8.3 × 10^{-7}		
N_2		298	[b]9.0 × 10^{-7}	8.3 × 10^{-7}	0.100[c]	0.979
N_2	0.51	308	6.3 × 10^{-7}	6.7 × 10^{-7}		
N_2	1.03	308	7.5 × 10^{-7}	6.7 × 10^{-7}		
N_2		308	[b]6.9 × 10^{-7}	6.7 × 10^{-7}	0.110[c]	0.985
CH_4	0.51	298	3.3 × 10^{-6}	3.1 × 10^{-6}		
CH_4	1.03	298	3.6 × 10^{-6}	3.1 × 10^{-6}		
CH_4		298	[b]3.5 × 10^{-6}	3.1 × 10^{-6}	0.085[c]	0.972
CH_4	0.51	308	2.6 × 10^{-6}	2.4 × 10^{-6}		
CH_4	1.03	308	2.7 × 10^{-6}	2.4 × 10^{-6}		
CH_4		308	[b]2.7 × 10^{-6}	2.4 × 10^{-6}	0.090[c]	0.972
CH_4	0.51	323	1.9 × 10^{-6}	1.6 × 10^{-6}		
CH_4	1.03	323	1.9 × 10^{-6}	1.6 × 10^{-6}		
CH_4		323	[b]1.9 × 10^{-6}	1.6 × 10^{-6}	0.110[c]	0.965
CO_2	0.51	298	2.1 × 10^{-5}	1.9 × 10^{-5}		
CO_2	1.03	298	2.4 × 10^{-5}	1.9 × 10^{-5}		
CO_2		298	[b]2.3 × 10^{-5}	1.9 × 10^{-5}	0.030[c]	0.980
CO_2	0.51	308	1.7 × 10^{-5}	1.3 × 10^{-5}		
CO_2	1.03	308	1.7 × 10^{-5}	1.3 × 10^{-5}		
CO_2		308	[b]1.7 × 10^{-5}	1.3 × 10^{-5}	0.043[c]	0.982
CO_2	0.51	323	1.2 × 10^{-5}	7.9 × 10^{-6}		
CO_2	1.03	323	1.2 × 10^{-5}	7.9 × 10^{-6}		
CO_2		323	[b]1.2 × 10^{-5}	7.9 × 10^{-6}	0.050[c]	0.962
CO_2	0.51	338	7.3 × 10^{-6}	4.9 × 10^{-6}		
CO_2	1.03	338	7.8 × 10^{-6}	4.9 × 10^{-6}		
CO_2		338	[b]7.6 × 10^{-6}	4.9 × 10^{-6}	0.070[c]	0.974

[a] Estimated with the Langmuir parameters in Table 3

[b] Average value for each pair of pulses

[c] Estimated by fitting the model to each pair of pulses simultaneously

$$v_0 = \frac{Q}{S_{bed}\varepsilon}\frac{T_{bed}}{T_{lab}} \tag{8}$$

where T_{bed} and T_{lab} are the bed and laboratory temperatures, respectively, S_{bed} is the bed cross-section. The mass balance in macropores is:

$$\frac{\partial c_{macro}}{\partial t} = \frac{3}{R_p\varepsilon_p}k_{macro}(c - c_{macro}) - \frac{3(1-\varepsilon_p)}{\varepsilon_p}\frac{D_c}{r_c^2}\frac{\partial q}{\partial x_r}\bigg|_{x_r=1} \tag{9}$$

where the second term in the RHS of Eq. (9) is the rate of adsorption in the $AlPO_4$-11 spherulites: D_c/r_c^2 is the diffusion time constant, x_r is the dimensionless radial coordinate in the spherulites, and q is the adsorbed concentration (in mol m^{-3}).

The following boundary conditions for Eq. (4) are employed:

$$x = 0 \quad v_0 c - \frac{D_L}{L}\frac{\partial c}{\partial x} = v_0 c_{T2} \tag{10}$$

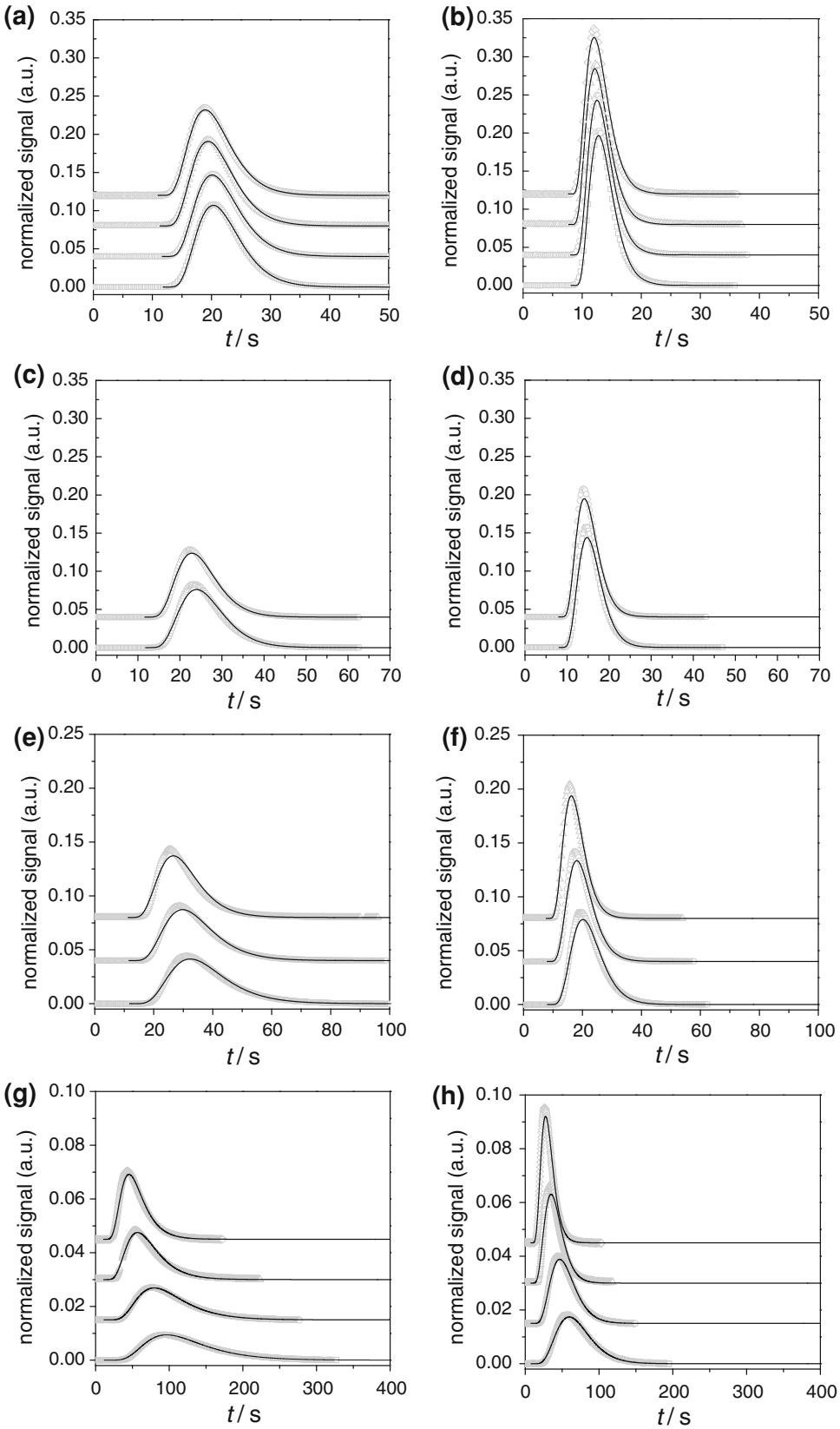

Fig. 6 Pulse responses from an $AlPO_4$-11 bed. *Grey symbols* are the experimental signal and *black lines* are the theoretical signal from the model. *Squares*, 25 °C; *circles*, 35 °C; *triangles*, 50 °C, *diamonds*, 65 °C. **a** Helium, $Q = 30.7$ ml min^{-1}. **b** Helium, $Q = 61.6$ ml min^{-1}. **c** Nitrogen, $Q = 30.7$ ml min^{-1}. **d** Nitrogen, $Q = 61.6$ ml min^{-1}. **e** Methane, $Q = 30.7$ ml min^{-1}, **f** Methane, $Q = 61.6$ ml min^{-1}. **g** Carbon dioxide, $Q = 30.7$ ml min^{-1}, **h** Carbon dioxide, $Q = 61.6$ ml min^{-1}

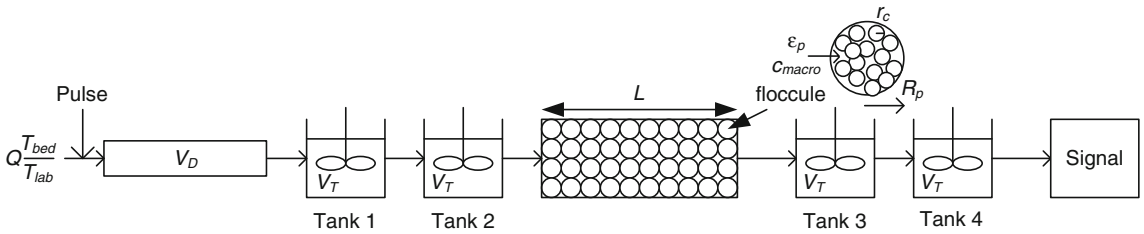

Fig. 7 Schematic representation of the flow pattern

$$x = 1 \quad \frac{\partial c}{\partial x} = 0 \tag{11}$$

where c_{T2} is the concentration in Tank 2 (Fig. 7). The mass balance in Tank 1 is:

$$\frac{dc_{T1}}{dt} = \frac{f_{pulse}(t) - v_0 S_{bed} \varepsilon c_{T1}}{V_T} \tag{12}$$

where $f_{pulse}(t)$ is the function describing the evolution of the injected gas flow during the pulse injection. It is assumed that the pulse does not change its shape as it crosses V_D (Fig. 7): The following pulse function was proposed:

$$f_{pulse}(t) = \frac{1}{5 \times 10^{-3}\sqrt{\pi}} \exp\left[-\left(\frac{t - 0.05}{5 \times 10^{-3}}\right)^2\right] \tag{13}$$

This function describes a normalized pulse with maximum flow of adsorptive at $t = 0.05$ s. The pulse is so narrow that the function parameters have a negligible effect on the simulated signal in the studied conditions. The mass balances in Tanks 2, 3 and 4 are:

$$\frac{dc_{T2}}{dt} = \frac{v_0 S_{bed} \varepsilon (c_{T1} - c_{T2})}{V_T} \tag{14}$$

$$\frac{dc_{T3}}{dt} = \frac{v_0 S_{bed} \varepsilon (c_{x=1} - c_{T3})}{V_T} \tag{15}$$

$$\frac{dc_{T4}}{dt} = \frac{v_0 S_{bed} \varepsilon (c_{T3} - c_{T4})}{V_T} \tag{16}$$

The mass balance in the spherulites is,

$$\frac{\partial q}{\partial t} = \frac{D_c}{r_c^2}\left(\frac{1}{x_r^2}\frac{\partial}{\partial x_r}\left(x_r^2 \frac{\partial q}{\partial x_r}\right)\right) \tag{17}$$

The boundary conditions for this equation are

$$\begin{aligned} x_r = 0 \quad & \frac{\partial q}{\partial x_r} = 0 \\ x_r = 1 \quad & q = K_c c_{macro} \end{aligned} \tag{18}$$

The initial condition is that the dependent variables are zero. The predicted normalized signal is calculated as follows:

$$N.S. = v_0 S_{bed} \varepsilon c_{T4} \tag{19}$$

The model is solved numerically using the PDECOL package (Madsen and Sincovec 1979), which uses orthogonal collocation on finite elements (OCFE) technique for the discretization of the axial coordinate. Hermite polynomials of third degree were used for the discretization of the radial coordinate in the particle (Finlayson 1980). The model is fitted to the experimental pulse responses by minimizing the sum of square residuals $=\sum \left(y_{\exp} - y_{\text{calc}}\right)^2$, where y is the normalized signal. The proportion of variance in the experimental data explained by the theoretical model was estimated with the coefficient of determination, $r^2 = 1 - \sum \left(y_{\exp} - y_{\text{calc}}\right)^2 / \sum \left(y_{\exp} - \overline{y_{\exp}}\right)^2$. For the helium pulses, the only adjustable parameter was V_T (Fig. 7). The value of V_D was calculated as a function of V_T, imposing that the first moment of the theoretical and the experimental pulse responses are the same. The required value of V_D is then calculated from the following equation:

$$V_D = Q\frac{T_{bed}}{T_{lab}}\left(\mu_{He} - \frac{L}{v_0}\left(1 + \frac{(1-\varepsilon)\varepsilon_p}{\varepsilon}\right) - \frac{4V_T}{Q\frac{T_{bed}}{T_{lab}}} - 0.05\,\text{s}\right) \tag{20}$$

where μ_{He} is the first moment of the fitted helium pulse. The theoretical pulses are displaced forward in time by the residence time in V_D ($V_D/(QT_{bed}/T_{lab})$). It was checked that the values of μ_{He} calculated with Eq. (2) from each displaced theoretical pulse and from the fitted experimental pulse are identical for any value of V_T. With this method, the value of V_T was estimated independently for each carrier gas flow rate and each temperature, resulting in values ranging between 1 and 1.25×10^{-6} m^3, with r^2 between 0.98 and 0.99 in all the pulses. A comparison between the theoretical and experimental helium pulse responses is given in Fig. 6a, b.

For estimating the value of D_c/r_c^2 for the adsorbing gases (nitrogen, methane and carbon dioxide), V_T and V_D are set to the values estimated for the helium pulse with the same carrier flow rate and temperature, and K_c is calculated with Eq. (3). Thus, D_c/r_c^2 is estimated independently, as it is the only adjustable parameter for the adsorbing gases.

The model was fitted to each pair of experimental pulse responses of adsorbing gases with different carrier gas flow

rate and constant temperature, imposing a constant value of D_c/r_c^2. The fitting results are given in Table 4, and a comparison between the experimental and theoretical pulses is presented in Fig. 6. It is observed that the model describes all the experimental pulses satisfactorily, with values of r^2 between 0.96 and 0.98, indicating that the model is able to explain most of the variance of the experimental pulses (96–98 %). However, it is observed that the experimental pulses are slightly narrower and sharper than the simulated curves. This small deviation (a 2–4 % of unexplained variance) probably comes from the relatively simple model used for describing the dispersion in the experimental installation, as this model affects the shape of all the pulses, and the same kind of deviation is systematically observed in all the pulses of the adsorbing gases.

All the simulated pulse responses were sensitive to the value of D_c/r_c^2, indicative of the mass transfer resistance inside the $AlPO_4$-11 spherulites. A reduction of D_c/r_c^2 with respect to the estimated values results in much broader peaks with a long tail which is not observed in the experiments. On the contrary, the simulated pulse responses were insensitive to R_p (even when it is increased 10 times). R_p is the radius of the adsorbent particles (floccules), which determines the combined influence of the external mass transfer resistance and the mass transfer resistance in the meso- and macroporosity [ε_p, Eqs. (4), (5), (9)]. On this basis, it is deduced that the estimated values of D_c/r_c^2 describe the diffusional resistance in the spherulites. It is important to note that the spherulites are polycrystalline aggregates, where the internal defects could have some effect on the intracrystalline mass transfer resistance. In the absence of literature data about diffusion parameters of the studied gases in $AlPO_4$-11 with other crystalline morphology, it is not possible to check this hypothesis.

The diffusion time constants for the three gases decrease in the order nitrogen > methane > carbon dioxide. It is deduced that the molecular size (methane > nitrogen > carbon dioxide) do not determine the mobility of this gases in the $AlPO_4$-11 material. The diffusion time constants increase with temperature moderately for the three gases in the studied temperature range. The estimated activation energy of diffusion is about 7 kJ mol^{-1} for nitrogen, 8 kJ mol^{-1} for methane, and about 16 kJ mol^{-1} for carbon dioxide. These low values indicate that the energy barriers for the diffusion of these adsorbates are small. This is consistent with the fact that all these adsorbates have molecular sizes smaller than the pore openings of $AlPO_4$-11, and that the pores do not contain cations which could hinder the diffusion process. The diffusion time constants increase as the adsorption energy decreases. According to the surface diffusion theory (Yang 2003), the mobility of an adsorbed molecule is inversely proportional to the average residence time of the molecule in the adsorption site. This time is proportional to $\exp(\Delta E/RT)$, where ΔE is the difference in energy between the lowest energy in the adsorption site and the state with free mobility. It is usually assumed that ΔE is a fraction (about a half) of the adsorption enthalpy (Suzuki 1990). As the order of adsorption enthalpies is carbon dioxide > methane > nitrogen, this theory explains the observed order of diffusion time constants, as they should be inversely proportional (approximately) to $\exp(0.5\Delta H/RT)$.

The diffusion coefficients were estimated from the diffusion time constants by assuming that the half diffusion length (r_c) is the radius of the aluminophosphate spherulites (taken as 3 μm, Fig. 4). At 298 K, the following values are obtained for nitrogen, methane and carbon dioxide, respectively: 9, 7.6 and 2.7×10^{-13} m^2 s^{-1}. The measured diffusivities have been compared with values reported in the literature for the same gases in other molecular sieves with different pore opening: 4A zeolite (0.38 nm), 5A zeolite (0.44 nm) and ZSM-5 (0.6 nm). The diffusivities in $AlPO_4$-11 follow the dependence on pore size expected intuitively, as they are higher than the ones reported at 298 K in 4A zeolite: 9.5×10^{-14} m^2 s^{-1} for nitrogen (Karger and Ruthven 1992); 5×10^{-15} m^2 s^{-1} for methane (Karger and Ruthven 1992); and 2.1×10^{-15} m^2 s^{-1} for carbon dioxide (Yang 2003). They are also lower than the ones measured in other zeolites at 298 K with larger pore openings: 1×10^{-10} m^2 s^{-1} for nitrogen in 5A zeolite (Karger and Ruthven 1992); 1.1×10^{-10} m^2 s^{-1} for methane in ZSM-5 (Ruthven 1984).

3.4 Potential performance of $AlPO_4$-11 in biogas upgrading by PSA

The potential performance of $AlPO_4$-11 in the upgrading of biogas by PSA has been evaluated by designing this process with a dynamic model which includes the adsorption equilibrium and kinetic parameters measured in this work. This model has already been employed in the separation of methane/nitrogen mixtures by a three-bed PSA with silicalite in a previous work (Delgado et al. 2011). The same PSA cycle has been used in this work because it predicted an efficient separation of a binary methane/nitrogen mixture with a similar proportion of gases as that of biogas.

The PSA cycle proposed consists of three beds passing through twelve consecutive steps. A scheme of the cycle is shown in Fig. 8a, and the sequence table is shown in Fig. 8b. Feed (biogas) at the high pressure in the cycle (P_H) is introduced in the first bed in Step I, and raffinate (methane-rich product) is produced. In Step II, a portion of the extract (carbon dioxide-rich product) is introduced as feed (rinse step), and more raffinate is produced. At the same time, the proportion of carbon dioxide in the bed is

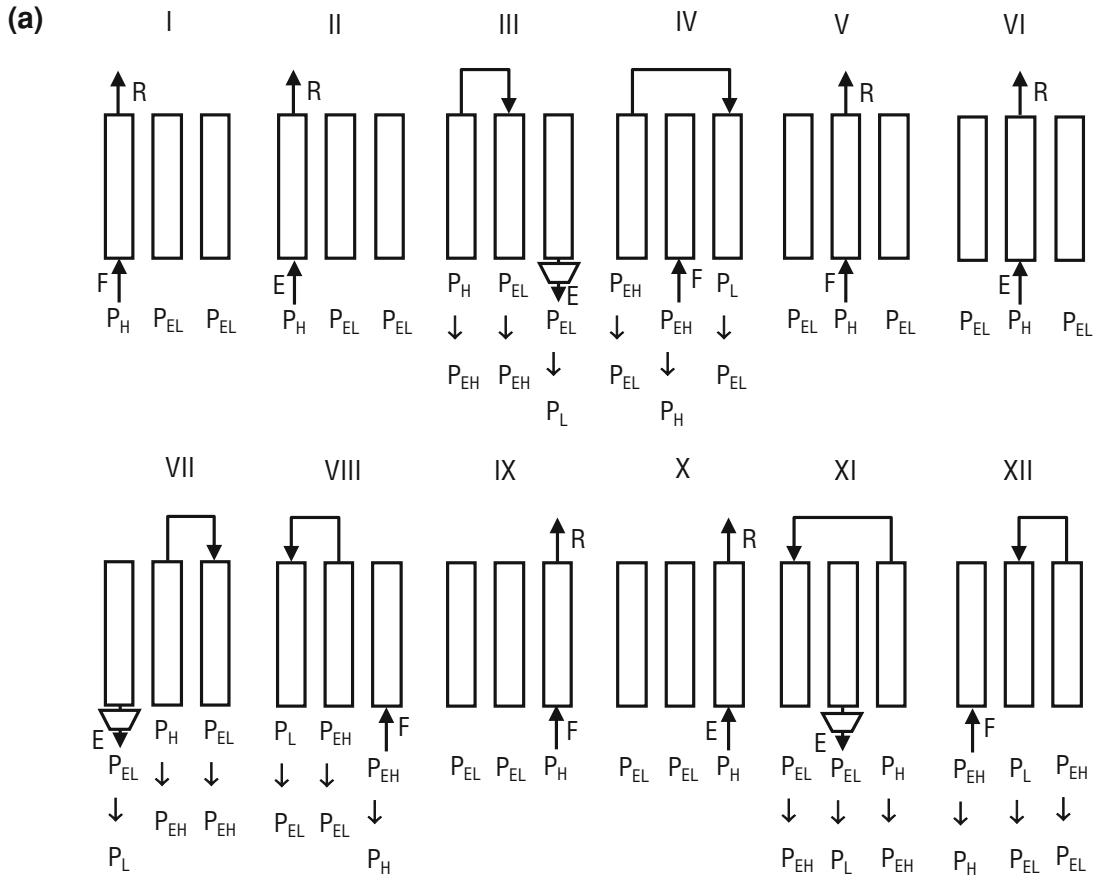

(b)

Step / Bed	I	II	III	IV	V	VI	VII	VIII	IX	X	XI	XII
Left	F	R	HDE	LDE	I	I	B	LPE	I	I	HPE	P
Middle	I	I	HPE	P	F	R	HDE	LDE	I	I	B	LPE
Right	I	I	B	LPE	I	I	HPE	P	F	R	HDE	LDE
t_{step}(s)	4	38	40	40	4	38	40	40	4	38	40	40

Fig. 8 **a** Scheme of the three-bed PSA cycle. P_L and P_H are the low and high pressures. P_{EL} and P_{EH} are the low and high equalization pressures ($P_L < P_{EL} < P_{EH} < P_H$). F, E and RF denote feed, extract (carbon dioxide-rich product) and raffinate (methane-rich product), respectively. **b** Sequence table for the three-bed cycle. *F* feed, *R* rinse, *HDE* high depressurizing equalization, *LDE* low depressurizing equalization, *I* idle, *B* blowdown, *LPE* low pressurizing equalization, *HPE* high pressurizing equalization, *P* pressurization

increased. In Step III, the first bed is equalized with the bed with low intermediate pressure (co-current equalization). At the same time, the other bed with low intermediate pressure is depressurized counter currently down to the low pressure (P_L) where the extract is obtained at 1 bar (blowdown). In Step IV, the first bed is equalized with the bed previously evacuated (a second co-current equalization step), and the other bed is pressurized with feed mixture up to the high pressure. The rest of the steps are the same for the other two beds.

The biogas is simulated as a binary carbon dioxide/methane mixture (50/50 v/v). It is assumed that the biogas is available at atmospheric pressure (100 kPa). One design specification is to produce methane with purity higher than 98 %, as the maximum allowable carbon dioxide content in natural gas is 2 % (Santos et al. 2011). Other desired design specification is to reach a carbon dioxide concentration in the extract above 93 %, the minimum purity to liquefy the extract by compression at ambient temperature (as estimated with AspenPlus®). This way, it can be sent to

Table 5 Model for a PSA process for separating carbon dioxide/methane mixtures with $AlPO_4$-11

Total mass balance $\varepsilon\frac{\partial C}{\partial t} = -\left(\frac{\partial u}{\partial z}C + u\frac{\partial C}{\partial z}\right) - (1-\varepsilon)\rho_p\sum_{i=1}^{i-n}\frac{d\bar{n}_i}{dt}$

Mass balance of ith component $\varepsilon\frac{\partial(Cy_i)}{\partial t} = -\frac{\partial}{\partial Z}(uCy_i) + D_L\varepsilon\frac{\partial}{\partial z}\left(C\frac{\partial y_i}{\partial z}\right) - (1-\varepsilon)\rho_P\frac{d\bar{n}_i}{dt}$

Equation of state $C = \frac{P}{RT}$

Momentum balance $-\frac{\partial P}{\partial z} = \frac{150\mu(1-\varepsilon)^2}{\varepsilon^3 4R_p^2}u + \frac{1.75(1-\varepsilon)\rho_g}{\varepsilon^3 2R_p}u^2$

Energy balance in the bed $\frac{\partial T}{\partial t} = \frac{\lambda\frac{\partial^2 T}{\partial Z^2} - uCc_{p,g}\frac{\partial T}{\partial z} + \sum_{i=1}^{i=n}(1-\varepsilon)\rho_p\frac{d\bar{n}_i}{dt}\left(-\Delta H_{ads,i}\right) + \varepsilon RT\frac{\partial C}{\partial t} - \frac{2}{R_i}h_w(T-T_w)}{\varepsilon Cc_{v,g} + (1-\varepsilon)\rho_p C_{p,s}}$

Energy balance in the column wall $\frac{\partial T_w}{\partial t} = \frac{2R_i h_w(T-T_w) - 2(R_i+l)h_{ext}(T_w - T_{ext})}{\rho_w C_{p,w}\left[(R_i+l)^2 - R_i^2\right]}$

Adsorption rate equation $\frac{d\bar{n}_i}{dt} = k_{s,i}\left(n_i^* - \bar{n}_i\right)$

Adsorption isotherm

Extended Langmuir equation including the gas in macropores $n_i^* = \frac{n_{\max j}b_i P y_i}{1+\sum_{j=1}^{j=n}b_i P y_i} + \frac{\varepsilon_{macro}}{\rho_p}\frac{P_{y_i}}{RT}$.

Van't Hoff equation $b_i = b_{0,i}\ \exp\left(\frac{-\Delta H_{ads,i}}{RT}\right)$

LDF mass transfer parameter of ith component $k_{s,i} = \left[\frac{R_p\rho_p n_{iF}}{3k_F\frac{Py_{iF}}{RT_F}} + \frac{R_p^2\rho_p n_{iF}\tau}{15\varepsilon_{macro}D_m\frac{Py_{iF}}{RT_F}} + \frac{r_c^2}{15D_c}\right]$

a sequestration process. The bed length and the feed gas velocity have been taken from our previous work (Delgado et al. 2011).

The dynamic model is based on the mass, energy and momentum balances, and model equations are presented in Table 5. Boundary and initial conditions can be found elsewhere (Delgado and Rodrigues 2008; Delgado et al. 2011). The Peclet numbers of mass and heat dispersion are set to 500 to approximate the usual plug flow assumption in industrial adsorption columns, as higher values had negligible effect on the performance. The extended Langmuir equation with the parameters of the pure components has been used to describe the adsorption isotherm of carbon dioxide-methane mixtures. This model has been selected because it is useful for practical design purposes (Yang 2003). The energetic heterogeneity of carbon dioxide adsorption, indicated by the lack of fit of the Langmuir equation at low pressures (enhancement in Fig. 5c), could have some effect on the separation performance. At the average temperature in the simulated process, 298 K, the experimental Henry's law constant is a 21 % larger than the one derived from the Langmuir model (Table 4). The deviation between the Langmuir model and the experimental data at 298 K starts to decrease for pressures above 2.5 kPa, becoming very small at 3.3 kPa. Assuming that two kinds of adsorption sites with different adsorption energy are available for carbon dioxide at pressures below 2.5 kPa, and that the most energetic ones are fully occupied at this pressure, the proportion of energetic sites with respect to all the sites (estimated as q/q_{max}) is 0.8 %. To consider the possible effect of the energetic heterogeneity on the simulated performance, a correction factor has been included to describe better the carbon dioxide adsorption isotherm in the range between 0 and 3.3 kPa, so that $b_{CO2new} = b_{CO2old}f(p_{CO2})$. The correction factor is:

$$f(p_{CO2}) = 1.21 + \frac{(1-1.21)}{1+\exp[-0.005(p_{CO2}-2500)]} \tag{21}$$

This factor was designed to change from 1.21 to 1 when the pressure is less or more than 2.5 kPa, becoming practically 1 at 3.3 kPa. The extended Langmuir equation with the parameters of the pure components (Table 3) has been used to describe the adsorption isotherm of carbon dioxide-methane mixtures, including the correction factor described previously. The bed properties used in the simulation are presented in Table 6. To simulate the properties of $AlPO_4$-11 pellets (not available), it has been assumed that the volume fractions of crystals, binder and voids in the column are the same as the ones measured experimentally in silicalite pellets in our laboratory. For pellets with 20 % w/w of binder, the volume distribution in the column is: voids between pellets = 40 %, crystals = 32.4 %, binder (dense) = 3.6 %, extracrystalline voids (in pellet) = 24 %. The crystal density of $AlPO_4$-11 is taken from Table 2. On this basis, the hypothetical pellet density (Table 6) used in the calculations has been estimated starting from the volume fractions measured experimentally for silicalite pellets:

$$0.324\frac{m^3_{crystals}}{m^3_{column}}\frac{m^3_{column}}{(1-0.4)m^3_{pellet}} = 0.54\frac{m^3_{crystals}}{m^3_{pellet}} \tag{22}$$

$$0.036\frac{m^3_{densebinder}}{m^3_{column}}\frac{m^3_{column}}{(1-0.4)m^3_{pellet}} = 0.06\frac{m^3_{densebinder}}{m^3_{pellet}} \tag{23}$$

Table 6 Model parameters used in the PSA design

Bed length	1 m
Bed diameter	0.2 m
Feed and external air temperature	298 K
High pressure	100 kPa
Low pressure	20 kPa
Pellet radius	5×10^{-4} m
Pellet macroporosity	0.4
Pellet tortuosity	3
Bed voidage between particles	0.4
Pellet density	1,645 kg m^{-3}
Weight fraction of binder	14.4 %
CO_2-CH_4 molecular diffusivity	1.8×10^{-5} m^2 s^{-1}
Heat and mass Peclet numbers	500
Adsorbent heat capacity	1,000 J kg^{-1}
Gas heat capacity at constant pressure	37 J kg^{-1} K^{-1}
Gas heat capacity at constant volume	28 J kg^{-1} K^{-1}
Gas viscosity	1.35×10^{-5} Pa s
Wall heat capacity	500 J kg^{-1} K^{-1}
Wall thickness	0.002 m
Wall density	8,000 kg m^{-3}
Gas to wall heat transfer coefficient[a]	60 W m^{-2} K^{-1}
Wall to air heat transfer coefficient[b]	2 W m^{-2} K^{-1}

[a] Taken from Da Silva and Rodrigues (2001)

[b] Estimated from a literature correlation for free convection in air (Holman 2010)

$$\text{pellet density} = \frac{0.06\text{m}^3_{\text{densebinder}} \times 3895 \frac{\text{kg}}{\text{m}^3_{\text{densebinder}}} + 0.54\text{m}^3_{\text{crystals}} 2611 \frac{\text{kg}}{\text{m}^3_{\text{crystals}}}}{1\ \text{m}^3_{\text{pellet}}} = 1645 \frac{\text{kg}}{\text{m}^3_{\text{pellet}}} \tag{24}$$

The weight fraction of $AlPO_4$-11 in the theoretical pellets is 85.6 %, which was considered in the simulations (the values of $n_{max,i}$ in the extended Langmuir equation were multiplied by 0.856). It is important to note that in this calculation it is assumed that separate spherulites of $AlPO_4$-11 are agglomerated to obtain the hypothetical pellets. It is also assumed that the separate spherulites pack in the pellets as silicalite crystals do. This, together with the presence of dense binder, explains the higher pellet density of the theoretical pellets with respect to the particle density measured experimentally for real $AlPO_4$-11 particles (floccules), where the spherulites pack more loosely.

The mass transfer coefficients between the gas and the adsorbent have been estimated with the expression proposed by Farooq and Ruthven (1990) (Table 6), which includes the external resistance, the resistance in macropores, and the resistance in micropores in series. The external mass transfer coefficient is estimated with Eq. (6), and the inverse of the diffusion time constants (r_c^2/D_c) of carbon dioxide and methane are taken from Table 4 at 298 K. The performance parameters (methane purity, recovery, productivity, power consumption) for one cycle at steady state were calculated with the following expressions:

$$\text{CH}_4 \text{ purity} = \frac{\text{moles of CH}_4 \text{ in raffinate}}{\text{moles of raffinate}} \tag{25}$$

$$\text{CH}_4 \text{ recovery} = \frac{\text{moles of CH}_4 \text{ in raffinate}}{\text{moles of feed}} \tag{26}$$

$$\text{CO}_2 \text{ purity} = \frac{\text{moles of CO}_2 \text{ in extract}}{\text{moles of extract}} \tag{27}$$

$$\text{Productivity} = \frac{\text{kg of CH}_4 \text{ in raffinate}}{(\text{cycle time})3(\text{kg of adsorbent in each bed})} \tag{28}$$

$$\text{Power consumption} = 3 \int_0^{t_m} \frac{(\text{flux at inlet in blowdown}) \pi R_1^2 \left(\frac{kRT_{inlet}}{(k-1)\eta_c} \left(\left(\frac{P_{atm}}{P_{inlet}} \right)^{\frac{k-1}{k}} - 1 \right) \right) dt}{\text{kg of methane in raffinate}} \tag{29}$$

where the raffinate is the sum of the products of the feed and rinse steps, and cycle time is 3 (duration step I) + 3 (duration step II) + 6 (duration step III). A value of $k = 1.3$ is taken for a carbon dioxide/methane mixture 95/4 (% v/v) (AspenPlus®), and $\eta_C = 0.8$ (Grande and Rodrigues 2007).

In order to meet the design specifications, four degrees of freedom were available in the model, namely, the low pressure in cycle (P_L in Fig. 8), and the duration of the feed, rinse and pressure change steps (t_I, t_{II} and t_{III} in Fig. 8). It was observed that the duration of the feed and rinse steps had a strong effect on the product purity requirements. An increase in the duration of the feed and rinse steps yielded a lower methane purity in the raffinate and higher carbon dioxide purity in the extract, as the carbon dioxide concentration wave advances more along the bed. A long enough rinse step was crucial to get a high carbon dioxide concentration in the extract. The duration of the pressure change steps had a positive effect on the methane and carbon dioxide purities, because the mass transfer resistance in these steps becomes less important as this duration increases. However, this time cannot be increased indefinitely, because the cycle productivity decreases. After testing numerous combinations for t_I, t_{II} and t_{III}, it was found that the desired specifications are achieved with the following combination: $P_L = 20$ kPa, $t_I = 4$ s, $t_{II} = 38$ s and $t_{III} = 40$ s. The performance

Table 7 Performance results for the proposed PSA cycle for separating a carbon dioxide/methane mixture with $AlPO_4$-11 (Fig. 8)

Methane purity in raffinate [% (v/v)]	98.3
Methane recovery (%)	94.1
Carbon dioxide purity in extract (%)	94.4
Productivity (kg_{CH4} kg^{-1} h^{-1})	0.006
Energy requirement (kWh kg^{-1})	0.27

results obtained with this combination are shown in Table 7. These results show that the proposed process can be advantageous over other alternatives, as it can theoretically recover methane from a carbon dioxide/methane mixture by PSA with high purity and recovery, without requiring feed compression, and a higher low pressure in the cycle with respect to other alternatives (10–12 kPa, Sircar et al. 1988; Grande and Rodrigues 2007). The productivity is lower than the one reported in the literature (0.006 vs. 0.088 kg_{CH4} kg^{-1} h^{-1}, Santos et al. 2011), due to the lower pressure ratio used in the cycle studied in this work (5 vs. 13), but the recovery is higher (94 vs. 88 %), and the process proposed in this work can operate with the feed gas at 1 bar and 298 K, whereas the reported process operates at 4 bar and 323 K. The estimated energy consumption is low as compared with the energy content of the methane product (0.27 vs. 13.7 kWh kg^{-1}).

4 Conclusions

Aluminophosphate molecular sieve $AlPO_4$-11 has been synthesized by microwave heating. The adsorption isotherms of nitrogen, methane and carbon dioxide on the synthesized material up to 110 kPa have been measured with a volumetric method. The adsorption capacities of each gas are not determined by the molecular size, but by the strength of interaction with the pore surface (carbon dioxide > methane > nitrogen). The equilibrium selectivity towards carbon dioxide in carbon dioxide/methane mixtures is quite high with respect to other adsorbents that do not contain cations. The isotherms of nitrogen and methane can be described very well with the Langmuir model in the whole studied pressure and temperature range, whereas the model deviates from the experimental data of carbon dioxide at low pressures (below 5 kPa), suggesting that the adsorbent is energetically heterogeneous for carbon dioxide at low loadings. The average adsorption heats of the three gases have been estimated with the Langmuir model.

The adsorption Henry's law constants and diffusion time constants of nitrogen, methane and carbon dioxide in the synthesized $AlPO_4$-11 material have been measured from pulse experiments. The adsorption Henry's law constants measured with this method compare very well with the ones obtained by the volumetric method for nitrogen and methane. For carbon dioxide, although they are of the same order of magnitude, the deviation is higher probably due to higher curvature of the carbon dioxide isotherm at lower pressures. The diffusion time constants of the three gases have been estimated by fitting the experimental pulse responses with a theoretical model describing the diffusional resistance in the synthesized material. The diffusion time constants for the three gases decrease in the order nitrogen > methane > carbon dioxide, indicating that the mobility of the adsorbates in the micropores is determined by adsorption affinity rather than by the molecular size. The estimated diffusivities show the expected dependence with the pore size when compared with the values reported in the literature in molecular sieves with different pore opening.

The feasibility of recovering methane from biogas by PSA using $AlPO_4$-11 as adsorbent has been evaluated with a dynamic model including the adsorption equilibrium and kinetic information measured in this work. The simulation results show that the proposed process could produce methane from carbon dioxide/methane mixtures with high purity and recovery, treating the feed at atmospheric pressure, with a significantly lower pressure ratio than the PSA processes based on 13X zeolite. Although the application of $AlPO_4$-11 to biogas upgrading is promising, more experimental work using actual $AlPO_4$-11 pellets in a multi-column PSA installation is required to verify the advantages of the proposed process in a real system.

References

Baerlocher, C.H., Meier, W.M., Olson, D.H.: Atlas of Zeolite Framework types, 5th edn. Elsevier, Amsterdam (2001)

Da Silva, F.A., Rodrigues, A.E.: Propylene/propane separation by vacuum swing adsorption using 13X zeolite. AIChE J. **47**, 341–357 (2001)

Delgado, J.A., Rodrigues, A.E.: Analysis of the boundary conditions for the simulation of the pressure equalization step in PSA cycles. Chem. Eng. Sci. **63**, 4452–4463 (2008)

Delgado, J.A., Uguina, M.A., Sotelo, J.L., Águeda, V.I., Gómez, P.: Numerical simulation of a three-bed PSA cycle for the methane/nitrogen separation with silicalite. Sep. Purif. Technol. **77**, 7–17 (2011)

Dunne, J.A., Mariwala, R., Rao, M., Sircar, S., Gorte, R.J., Myers, A.L.: Calorimetric heats of adsorption and adsorption isotherms. 1. O_2, N_2, Ar, CO_2, CH_4, C_2H_6, and SF_6 on silicalite. Langmuir **12**, 5888–5895 (1996)

Dwivedi, P.N., Upadhyay, S.N.: Particle-fluid mass transfer in fixed and fluidized columns. Ind. Eng. Chem. Process Des. Dev. **16**, 157–165 (1977)

Farooq, S., Ruthven, D.M.: Heat effects in adsorption column dynamics. 1. Comparison of one- and two-dimensional models. Ind. Eng. Chem. Res. **29**, 1076–1084 (1990)

Finlayson, B.A.: Nonlinear analysis in chemical engineering. McGraw Hill, New York (1980)
Fu, L., Zhai, J.P., Hu, J.M., Li, I.L., Ruan, S.C., Tang, Z.K.: Synthesis of large silicon substituted $AlPO_4$-11 single crystals. Micropor. Mesopor. Mat. **137**, 1–7 (2011)
Grande, C.A., Rodrigues, A.E.: Biogas to fuel by vacuum pressure swing adsorption I. Behavior of equilibrium and kinetic-based adsorbents. Ind. Eng. Chem. Res. **46**, 4595–4605 (2007)
Holman, J.P.: Heat Transfer, 10th edn. McGraw Hill, Boston (2010)
Karger, J., Ruthven, D.M.: Diffusion in zeolites and other microporous solids. Wiley, New York (1992)
Lok, B.M, Messina, C.A., Patton, R.L., Gajek, R.T., Cannan, T.R., Flanigen, E.M.: Crystalline silicoaluminophosphates. U.S. Patent 4,440,871 (1984)
Lucena, S.M.P., Pereira, J.A.F.R., Cavalcante, C.L.: Structural analysis and adsorption sites of xylenes in $AlPO_4$-5 and $AlPO_4$-11 using molecular simulation. Micropor. Mesopor. Mat. **88**, 135–144 (2006)
Madsen, N.K., Sincovec, R.F.: Algorithm 540: PDECOL, general collocation software for partial differential equations [D3]. ACM Trans. Math. Soft. **5**, 326–351 (1979)
Predescu, L., Tezel, F.H., Chopra, S.: Adsorption of nitrogen, methane, carbon monoxide, and their binary mixtures on aluminophosphate molecular sieves. Adsorption **3**, 7–25 (1997)
Ruthven, D.M.: Principles of Adsorption and Adsorption Processes. Wiley, New York (1984)
Santos, M.S., Grande, C.A., Rodrigues, A.E.: New cycle configuration to enhance performance of kinetic PSA processes. Chem. Eng. Sci. **66**, 1590–1599 (2011)
Sircar, S., Kumar, R., Koch, W.R., VanSloun, J.: Recovery of methane from landfill gas. U.S. Patent 4,770,676 (1988)
Suzuki, M.: Adsorption Engineering. Kodansha, Tokyo (1990)
Valenzuela, D.P., Myers, A.L.: Adsorption equilibrium data handbook. Prentice Hall, New Jersey (1989)
Walendziewski, J., Pniak, B.: Synthesis, physicochemical properties and hydroisomerization activity of SAPO-11 based catalysts. Appl. Catal. A **250**, 39–47 (2003)
Wang, Q., Chen, G., Xu, S.: Hierarchical architecture observed in microspheres comprising microporous $AlPO_4$-11 nanocrystals. Micropor. Mesopor. Mat. **119**, 315–321 (2009)
Wilke, A.C.: Biogas: a renewable biofuel, Biogas use, http://biogas.ifas.ufl.edu/. Accessed Nov 2012 (2012)
Wilson, S.T., Lok, B.M., Messina, C.A., Cannan, T.R., Flanigen, E.M.: Aluminophosphate molecular sieves: a new class of microporous crystalline inorganic solids. J. Am. Chem. Soc. **104**, 1146–1147 (1982a)
Wilson, S.T., Lok, B.M., Flanigen, E.M.: Crystalline metallophosphate compositions. U.S. Patent 4, 310,440 (1982b)
Yang, R.T.: Adsorbents: Fundamentals and Applications. Wiley, New Jersey (2003)
Zhang, D., Li, W., Liu, Z., Xu, R.: Molecular simulation of methane adsorption in aluminophosphate molecular sieve $AlPO_4$-11. J. Mol. Struc.-THEOCHEM **804**, 89–94 (2007)
Zhu, G., Qiu, S., Gao, F., Wu, G., Wang, R., Li, B., Fang, Q., Li, Y., Gao, B., Xu, X., Terasaki, O.: Synthesis of aluminophosphate molecular sieve $AlPO_4$-11 nanocrystals. Micropor. Mesopor. Mat. **50**, 129–135 (2001)
Zhu, Z.D., Hartmann, M., Kevan, L.: Catalytic conversion of methanol to olefins on SAPO-n ($n = 11$, 34, and 35), CrAPSO-n, and Cr − SAPO-n molecular sieves. Chem. Mater. **12**, 2781–2787 (2000)